Orientation of α-Neurotoxin at the Subunit Interfaces of the Nicotinic Acetylcholine Receptor†

Siobhan Malany,‡ Hitoshi Osaka,‡,§ Steven M. Sine,|| and Palmer Taylor*,‡

Department of Pharmacology, 0636, University of California at San Diego, La Jolla, California 92093, and Receptor Biology Laboratory, Department of Physiology and Biophysics, Mayo Foundation, Rochester, Minnesota 55905

Received August 3, 2000; Revised Manuscript Received October 14, 2000

ABSTRACT: The α-neurotoxins are three-fingered peptide toxins that bind selectively at interfaces formed by the α subunit and its associating subunit partner, γ, δ, or ϵ of the nicotinic acetylcholine receptor. Because the α-neurotoxin from *Naja mossambica mossambica* I shows an unusual selectivity for the $\alpha\gamma$ and $\alpha\delta$ over the $\alpha\epsilon$ subunit interface, residue replacement and mutant cycle analysis of paired residues enabled us to identify the determinants in the γ and δ sequences governing α-toxin recognition. To complement this approach, we have similarly analyzed residues on the α subunit face of the binding site dictating specificity for α-toxin. Analysis of the $\alpha\gamma$ interface shows unique pairwise interactions between the charged residues on the α-toxin and three regions on the α subunit located around residue Asp^{99}, between residues Trp^{149} and Val^{153}, and between residues Trp^{187} and Asp^{200}. Substitutions of cationic residues at positions between Trp^{149} and Val^{153} markedly reduce the rate of α-toxin binding, and these cationic residues appear to be determinants in preventing α-toxin binding to α2, α3, and α4 subunit containing receptors. Replacement of selected residues in the α-toxin shows that Ser^8 on loop I and Arg^{33} and Arg^{36} on the face of loop II, in apposition to loop I, are critical to the α-toxin for association with the α subunit. Pairwise mutant cycle analysis has enabled us to position residues on the concave face of the three α-toxin loops with respect to α and γ subunit residues in the α-toxin binding site. Binding of *Nmm*I α-toxin to the $\alpha\gamma$ interface appears to have dominant electrostatic interactions not seen at the $\alpha\delta$ interface.

For the past 30 years, the α-neurotoxin family of snake venoms has served as primary tools for the pharmacological characterization of the nicotinic acetylcholine receptor (nAChR)[1] (*1*−*3*). The various subtypes of α-neurotoxins active on muscle receptors can be classified in two general categories: short (60−62 amino acids and 4 disulfide bonds) or long (66−74 amino acids and 5 disulfide bonds) (*4*). Toxins of both categories interact with receptors containing α1, β, $\gamma(\epsilon)$, and δ subunits found in skeletal muscle, while the long neurotoxins also bind to α7 containing receptors found in neuronal tissues (*5*).

α-Neurotoxins competitively inhibit agonist binding to the muscle nAChR by forming a high affinity, slowly dissociating complex through association at the $\alpha\gamma$ and $\alpha\delta$ subunit interfaces. The high affinity presumably results from the large van der Waals interfacial contact area (800−1200 Å^2) that the three fingered α-toxins exhibit in peptide−protein complexes (*6*−*8*). The contact zone potentially extends over much of the surface of the three α-toxin loops, which are held together by a disulfide-linked globular core. Extensive mutagenesis studies with erabutoxin (Ea), a member of the short toxin family, have delineated key residues in the α-toxin that stabilize the high affinity complex (*6*). The α-neurotoxin from *Naja mossambica mossambica* I (*Nmm*I) shares 60% sequence identity with Ea and, due to its high selectivity for the $\alpha\gamma$ subunit interface over that formed by $\alpha\epsilon$ (*9*), has served as a unique probe in our efforts to map the subunit binding interfaces of the muscle nAChR.

The nAChR in muscle is composed of four homologous subunits arranged in a pentamer of composition $\alpha_2\beta\delta\gamma$ (fetal) or $\alpha_2\beta\delta\epsilon$ (adult); agonists and competitive antagonists bind at interfaces between the $\alpha\delta$ and $\alpha\gamma$ ($\alpha\epsilon$) subunit pairs (*3*, *10*−*12*). Affinity labeling and site-specific mutagenesis studies of nAChR have identified key regions contributing to agonist binding, including three segments in the α subunit: residues surrounding Tyr^{93} and residues between Trp^{149} and Gly^{153} and between His^{186} and Asp^{200}; and four segments in the γ subunit (and corresponding residues on the δ subunit), including residues surrounding Lys^{34} and residues between Trp^{55} and Gln^{59}, Ser^{111} and Leu^{119}, and Phe^{172} and Glu^{176} (*2*, *11*−*13*).

Previously, we reported on the importance of residues 188−200 in the α subunit as a binding domain for *Nmm*I α-toxin recognition (*14*). We further examined charged substitutions on both the α subunit of nAChR and *Nmm*I and analyzed the energetics of binding and specificity for the combination of double mutations by thermodynamic mutant cycle analysis (*15*), a powerful technique for delin-

† Supported by United States Public Health Service Grants GM 18360 (to P.T.) and NS 31744 (to S.M.S.), a Uehara Memorial Foundation Fellowship (to H.O.), and a California Tobacco Related Diseases Fellowship (to S.M.).

* To whom correspondence should be addressed. Phone: (858)534-1366. Fax: (858)534-8248. E-mail: pwtaylor@ucsd.edu.

‡ University of California at San Diego.

§ Present address: Department of Degenerative Neurological Diseases, National Institute of Neuroscience, National Center of Neurology and Psychiatry, Kodaira, Tokyo 187-8502, Japan.

|| Mayo Foundation.

[1] Abbreviations: nAChR, nicotinic acetylcholine receptor; *Nmm*I, *Naja mossambica mossambica* I; α-BgTx, α-bungarotoxin; Ea, erabutoxin a.

10.1021/bi001825o CCC: $19.00 © 2000 American Chemical Society
Published on Web 11/18/2000

eating pairwise residue interactions that stabilize high affinity complexes (*16*−*18*). More recently, we have shown that Trp[55], Leu[119], Asp[174] and Glu[176] in the γ subunit likewise reside at the α-toxin binding interface (*19*, *20*). Double mutant cycle analyses of our combined investigations of determinants in the γ subunit have revealed that residues of loop II *Nmm*I toxin, Arg[33] and Lys[27], are primary points of contact for binding to the γ subunit face of the receptor binding site (*20*).

Structurally equivalent residues on both short and long α-neurotoxins, notably Ea and α-cobratoxin, respectively, recognize a similar region on the *Torpedo* receptor α subunit (*21*, *22*). In addition, Michalet et al. (*23*) recently determined by chemical cross-linking studies the relative proximities of the *Naja nigricollis* α-toxin mutant Q10C, K27C, W29C, R33C, and K47C to thiols Cys[192]−Cys[193] in the α subunit, specifically at the αγ site of *Torpedo* receptor.

Results from our laboratory and others have provided an initial view of the molecular interactions stabilizing the α-toxin−receptor complex. Still, the orientation of the α-toxin with respect to the αγ and αδ subunit interfaces remains to be established. Here, we extend our study of α-neurotoxin positioning at the subunit interfaces of the nAChR by analyzing interactions between a set of point charges on the α-toxin with an extended array of point charges on the α subunit. The present work reveals that Asp[99] and Trp[149] on the α subunit, in addition to residues Val[188], Tyr[190], Tyr[198], and Asp[200] (a binding region extending from position 186 to position 200), contribute significantly to *Nmm*I binding. Correspondingly, on the α-toxin, Ser[8] on loop I; Lys[27], Arg[33], and Arg[36] on loop II; and Lys[47] and Lys[48] on loop III are critical residues involved in the multipoint attachment to nAChR. These results, combined with our previous investigation of energetic linkages between α-toxin residues with the γ subunit, provide a refined picture of how *Nmm*I orients with respect to the α and γ subunit interfaces at the αγ site.

MATERIALS AND METHODS

Materials. α-Conotoxin MI was purchased from American Peptide Co. [125]I-Labeled α-bungarotoxin (α-BgTx) (specific activity ∼16 μCi/μg) was a product of NEN Life Science Products.

NmmI Expression and Purification. A cDNA encoding *Nmm*I α-toxin was subcloned into pEZZ-18 vector containing a coding sequence for two IgG binding proteins from Staphylococcal protein A. Mutations were constructed by bridging two restriction sites with synthetic double-stranded oligonucleotides. Staphylococcal protein A−*Nmm*I fusion protein was expressed using *Escherichia coli* HB 101, cleaved by CNBr and purified as described (*14*).

Construction of Mutant nAChRs. cDNAs encoding mouse nAChR subunits were subcloned into a cytomegalovirus-based expression vector, pRBG4. All mutations were introduced using the Quick Change site-directed mutagenesis kit (Stratagene, San Diego, CA) or by bridging the two introduced or natural restriction sites with double-stranded oligonucleotides. Chimeras were also constructed by bridging natural or introduced restriction sites. After the ligation of the fragments containing the mutated site or synthesized oligonucleotide into the original pRBG4 vector, the subcloned cassette was fully sequenced by the dideoxy method.

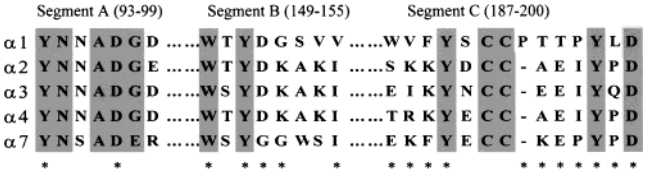

FIGURE 1: Alignment of extracellular regions forming the ligand binding site of the muscle (mouse) (α1) and the neuronal (rat) (α2, α3, α4, and α7) subunits of nAChR. The three segments on the α subunit face are designated A−C. Conserved residues are shaded. Asterisks indicate positions of studied residue mutations.

Cell Transfections. cDNAs encoding the wild-type and mutant subunits were transfected into human embryonic kidney (HEK-293) cells using $Ca_3(PO_4)_2$ in the ratios of α (15 μg)/β (7.5 μg)/δ (7.5 μg)/γ (7.5 μg). In cases where measured expression was low, higher expression levels were achieved by lowering the incubation temperature from 37 to 31 °C 24 h after transfection of the HEK cells and 36 h prior to harvesting.

Ligand Binding Measurements. Cells were harvested in phosphate-buffered saline, pH 7.4, containing 5 mM EDTA 2−3 days after transfection. They were briefly centrifuged, resuspended in K^+-Ringer's buffer, and divided into aliquots for binding assays. Specified concentrations of *Nmm*I were added to the samples 5 h prior to addition of [125]I-labeled α-bungarotoxin and measurement of the rate of association of labeled toxin with the nAChR. Dissociation constants (K_D values) of the ligands were determined from their capacity to compete with the initial rate of [125]I-labeled α-bungarotoxin association (*24*, *25*). A two-site analysis was used to ascertain dissociation constants at the αγ and αδ interfaces. Binding assays for all mutant *Nmm*I with wild-type nAChR and all mutant nAChR with wild-type *Nmm*I were conducted in the absence and presence of appropriate concentrations of α-conotoxin MI to block *Nmm*I binding at the αδ interface, when the distinction in *Nmm*I binding to the αδ and αγ interfaces was not obvious (*14*, *15*).

RESULTS

Residue Substitution at the α1 Subunit Binding Site. Three distinct segments in the mouse α subunit sequence [encompassing residues between 93 and 99 (segment A),[2] between 149 and 155 (segment B), and an extended region of residues between 186 and 200 (segment C)] contribute to ligand specificity as characterized by affinity labeling studies and site-specific mutagenesis (Figure 1) (*13*, *26*). Our previous investigations identified a critical region for *Nmm*I α-toxin recognition within segment C, defined by α residues Val[188], Tyr[190], Pro[197], and Asp[200] (*14*). To further explore individual residues on the αδ and αγ subunit interfaces that potentially contribute to the α-toxin−receptor interaction, we have constructed new substitutions at Asp[99] in segment A, at Trp[149] in segment B, and at Tyr[198] in segment C and examined their influence on *Nmm*I binding (Table 1, Figure 2). Mutant *Nmm*I α-toxins often bind with different affinities to the αδ

[2] To avoid confusion with the α-toxin loops that carry Roman numeral designations, we have defined these segments on the respective subunits by letters extending from the N-terminus: i.e., αA, αB, and αC and γA, γB, γC, and γD for the corresponding regions on the α and γ subunit faces that contribute to the binding site.

Table 1: Mutant Cycle Analysis for the α1 Subunit of the Nicotinic Acetylcholine Receptor and *Naja mossambica mossambica* Toxin[a]

mutations		binding energy K_D (nM)		binding energy ΔΔ*G*		coupling energy ΔΔG_{INT}	mutations		binding energy K_D (nM)		binding energy ΔΔ*G*		coupling energy ΔΔG_{INT}
receptor	toxin	αγ	αδ	αγ	αδ	αγ	receptor	toxin	αγ	αδ	αγ	αδ	αγ
WT	E10R	0.1	0.1	−0.2	−0.2		Y190T	WT	69	6.8	3.7	2.3	
WT	S8T	20	1.4	2.7	1.3		Y190T	E10R	2.4	2.4	1.7	1.7	**−1.8**
WT	S8E	1600	25	5.5	3.1		Y190T	S8E	13000	ND	6.8		**−2.4**
WT	S8K	330	11	4.6	2.6		Y190T	S8K	7750	ND	6.5		**−1.8**
*WT	K27E	54	1.8	3.5	1.5		*Y190T	K27E	2900	100	5.9	4.0	−1.3
*WT	R33E	2200	95	5.7	3.9		*Y190T	R33E	64000	9800	7.7	6.6	**−1.7**
WT	R36E	1950	50	5.5	3.5		Y190T	R36E	5000	5000	6.2	6.2	**−3.1**
*WT	K47A	1.5	1.5	1.4	1.4		Y190T	K47E	10000	1000	6.6	5.2	−0.4
WT	K47E	38	0.3	3.2	0.4		Y190T	K48E	92.0	9.1	3.8	2.5	−1.2
WT	K48E	1.4	0.2	1.3	0.2		Y198E	WT	12.5	0.2	2.7	0.2	
D99R	WT	2.5	0.1	1.7	−0.2		Y198E	E10R	2.0	0.2	1.6	0.1	−0.9
D99R	E10R	0.2	0.1	0.2	−0.2	−1.3	Y198E	S8E	50000	ND	7.6		−0.6
D99R	S8E	2300	13	5.7	2.7	−1.2	Y198E	S8K	4000	91	6.1	3.8	−1.2
D99R	S8K	3000	35	5.9	3.3	−0.1	Y198E	K27E	6000	4.5	6.3	2.1	0.1
D99R	K27E	1000	75	5.3	3.7	0.4	Y198E	R33E	26000	900	7.2	5.2	-1.2
D99R	R33E	6300	90	6.3	3.8	−0.8	Y198E	R36E	300000	ND	8.6		0.3
D99R	R36E	4900	95	6.2	3.9	−0.9	Y198E	K47E	2000	260	5.7	4.4	−0.3
D99R	K47E	33	3.0	3.2	1.8	**−1.5**	Y198E	K48E	170	4.2	4.2	2.0	0.2
D99R	K48E	0.4	0.4	0.7	0.7	**−2.1**	Y198R	WT	20	20	2.9	2.9	
W149K	WT	6.0	0.2	2.2	0.2		Y198R	E10R	24	0.7	3.0	1.0	0.3
W149K	E10R	0.6	0.6	0.9	0.9	−1.2	Y198R	S8E	>100000	ND	>8.0		−0.4
W149K	S8E	27000	ND	7.2		−0.5	Y198R	S8K	>1mM	ND	>9.3		**>1.8**
W149K	S8K	8000	2.0	6.5	1.6	−0.3	Y198R	K27E	2700	2700	5.8	5.8	−0.6
W149K	K27E	3200	24	5.9	3.0	0.2	Y198R	R33E	2000	120	5.7	4.0	**−3.0**
W149K	R33E	2000	30	5.7	3.1	**−2.3**	Y198R	R36E	85000	ND	7.9		−0.7
W149K	R36E	13000	40	6.8	3.3	−1.1	Y198R	K47E	300	30	4.6	3.2	**−1.7**
W149K	K47E	200	8	4.3	2.4	−1.2	Y198R	K48E	470	30	4.8	3.2	0.5
W149K	K48E	13.0	0.3	2.7	0.5	−0.9	D200K	WT	35	1.0	3.3	1.2	
V188D	WT	2.7	0.1	1.8	−0.2		D200K	E10R	7.9	0.6	2.4	0.8	−0.7
V188D	E10R	0.4	0.4	0.6	0.6	−0.9	D200K	S8E	16000	4100	6.9	6.1	**−1.9**
V188D	S8E	33500	2900	7.3	5.9	0.1	D200K	S8K	25000	1600	7.1	5.5	−0.7
V188D	S8K	5500	370	6.3	4.7	−0.1	D200K	K27E	1000	2	5.2	1.6	**−1.5**
*V188D	K27E	1600	54	5.5	3.5	0.3	D200K	R33E	11800	750	6.7	5.1	**−2.3**
*V188D	R33E	>500000	6200	>8.9	6.3	**>1.5**	D200K	R36E	38000	2250	7.4	5.7	**−1.5**
V188D	R36E	8100	325	6.5	4.6	−0.9	D200K	K47E	1500	90	5.5	3.8	−1.1
V188D	K47E	600	23	4.9	3.0	−0.1	D200K	K48E	150	7.0	4.1	2.3	−0.5
V188D	K48E	31	0.6	3.2	0.8	0.1	D200Q	WT	9.2	0.3	2.5	0.5	
V188K	WT	55	2.8	3.5	1.8		D200Q	E10R	2.6	0.3	1.7	0.5	−0.5
V188K	E10R	43	1.2	3.4	1.3	0.1	D200Q	S8E	16000	340	6.9	4.6	−1.1
V188K	S8E	119000	ND	8.1		−1.0	D200Q	S8K	2700	180	5.8	4.2	−1.2
V188K	S8K	38000	ND	7.4		−0.7	*D200Q	K27E	3200	49	5.9	3.5	−0.1
*V188K	K27E	5700	205	6.3	4.3	−0.6	*D200Q	R33E	31000	400	7.3	4.7	−0.9
*V188K	R33E	63000	1300	7.7	5.4	**−1.5**	D200Q	R36E	300000	26	8.6	3.1	0.5
V188K	R36E	2600	185	5.8	4.3	**−3.4**	D200Q	K47E	2100	25	5.7	3.1	−0.1
V188K	K47E	4300	60	6.1	3.6	−0.7	D200Q	K48E	100	1.1	3.9	1.2	0.1
V188K	K48E	375	7.1	4.7	2.3	−0.2							
Y190F	WT	70	2.8	3.7	1.8								
Y190F	E10R	14	1.1	2.7	1.2	−0.8							
Y190F	S8E	18000	ND	7.0		**−2.2**							
Y190F	S8K	82500	ND	7.9		−0.4							
*Y190F	K27E	44000	500	7.5	4.9	0.3							
*Y190F	R33E	390000	4500	8.8	6.1	−0.6							
Y190F	R36E	7900	7850	6.5	6.5	**−2.9**							
Y190F	K47E	2900	1300	5.9	5.4	−1.1							
Y190F	K48E	495	44.5	4.8	3.4	−0.2							

[a] Dissociation constants were determined from competition with the initial rate of the ^{125}I-labeled α-bungarotoxin binding. Receptors were expressed as $\alpha_2\beta\gamma\delta$ by transfection of the cDNAs encoding the respective sets of subunits. K_D values are dissociation constants for αδ and αγ sites by fitting a two-site analysis. Ratios of dissociation constants of mutant (mt) to wild type (wt) were calculated using an average or mean value of two or more measurements involving separate transfections. ΔΔ*G* is free energy of binding in kcal/mol calculated from the K_D as follows: $\Delta\Delta G = RT \ln(K_{D,mt}/K_{D,wt})$. ΔΔ$G_{INT}$, in kcal/mol, denotes a coupling free energy. An asterisk (*) indicates data of Ackermann et al. (*15*). ND, not determined because of low affinity. Bold letters denote a significant change in ΔΔG_{INT}.

and αγ interfaces (*14*, *15*). To distinguish the K_D values for the two sites, experiments were conducted in the presence and absence of α-conotoxin M1, which has 10 000-fold greater affinity for the αδ site over that formed at the αγ interface. Therefore, the measured K_D in the presence of α-conotoxin M1 should reflect α-toxin binding to the αγ subunit interface (*14*, *15*).

Substitutions in Segments A and B. Position 99 in segment A is a conserved anionic residue in both neuronal and muscle receptor α subunits, except in α7, that contains a cationic

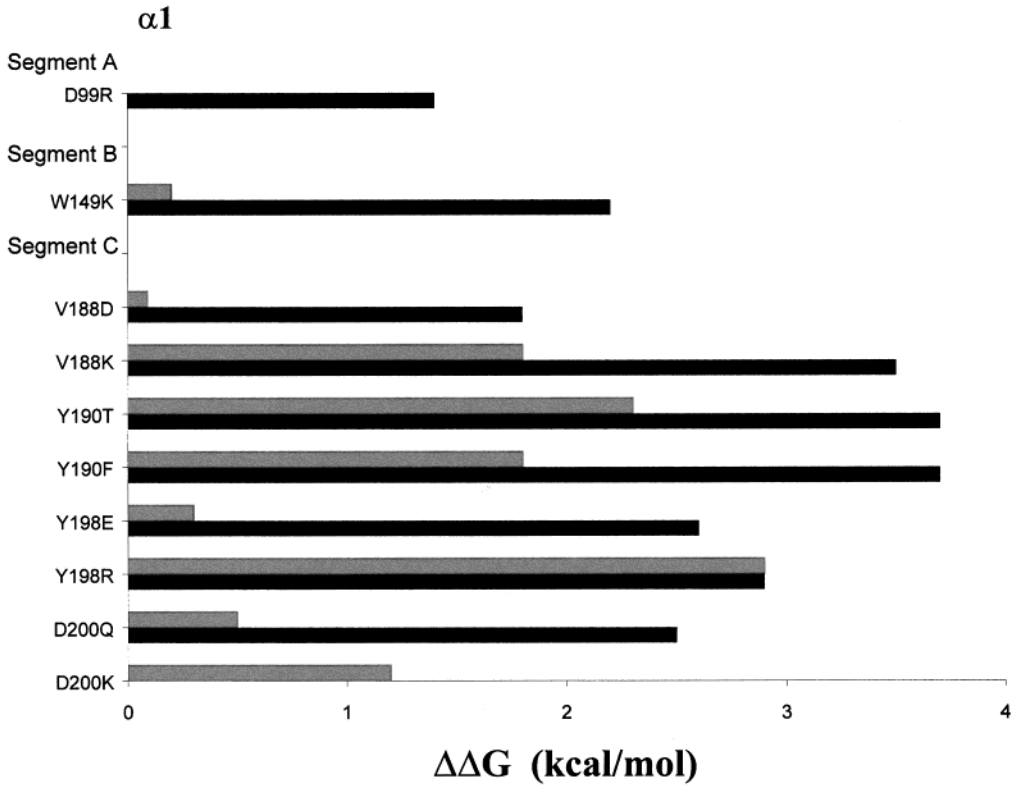

FIGURE 2: Mutagenesis of residues in segments A−C of the α1 subunit binding face of nAChR. ΔΔ*G* values given in Table 1 are compared in the figure for each mutant at the αγ site in black and at the αδ site in gray. The horizontal bars indicate ΔΔ*G* values obtained from comparing the ratios of K_D values for *Nmm*I with mutant and wild-type α1 subunits.

residue. We constructed the negative to positive charge substitution at this position, αD99R, which resulted in a modest affinity decrease (<2 kcal/mol) for *Nmm*I binding at the αγ site. Introduction of a positive charge for the conserved tryptophan at position 149 in segment B, αW149K, showed a larger affinity decrease (2.2 kcal/mol) at the αγ site. Expression was not detectable for the αW149E mutant.

Substitutions in Segment C. Of the key residues we have examined in segments A−C of the α subunit, the greatest contributions toward binding α-toxin are found in segment C (Figure 2). Substitution for the tyrosine at α190 by either phenylalanine or threonine results in substantial losses in affinity at both sites but predominately at the αγ site. Likewise, the αV188K and αD200K mutations display nearly equivalent losses in affinity at the αγ site. Substitution for the conserved tyrosine at position α198 with a positive charged side chain, Y198R, decreased *Nmm*I affinity by ~3.0 kcal/mol at both the αδ and αγ sites; whereas, a negative charge substitution at this position, Y198E, decreased affinity by the same magnitude only at the αγ site.

Influence of Segment B Residues on α*-Bungarotoxin* (α*-BgTx*) *Binding.* Several mutations in the α subunit, when transfected with β, γ, and δ subunits, exhibited expression levels too low for binding studies of the short α-toxin, *Nmm*I. Substitution of Lys for Leu[199] and His[204] in the α subunit did not yield expression of receptor on the cell surface. The equivalent positions on the α3 subunit are determinants for neuronal bungarotoxin binding to α3β2 receptors (*27*). Furthermore, the following α mutations in segment B gave low or nondetectable expression levels: D152K, G153D, G153K, S154A, V155K, V155D, and V156I. These residue positions constitute a highly conserved region on neuronal

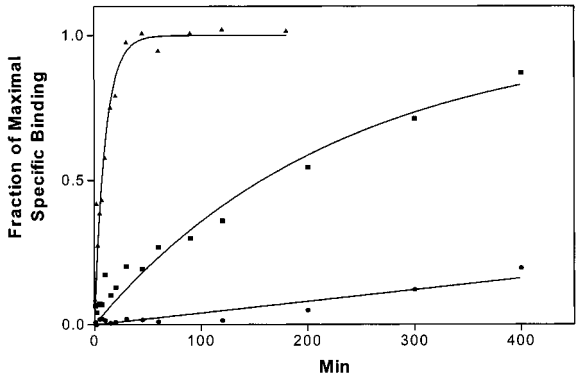

FIGURE 3: Kinetics of ^{125}I-labeled α-bungarotoxin association with mouse wild-type and mutant nAChRs. Association of 20nM ^{125}I-labeled α-bungarotoxin with 200 pM wild-type (▲), αG153K (■), and αV155K (●) mutant receptors. Data are fit by a single-exponential approach to equilibrium with k_{on} of $4.0 \pm 0.5 \times 10^6$ M^{-1} min^{-1} for wild-type, $2.0 \pm 0.5 \times 10^5$ M^{-1} min^{-1} for αG153K, and ~2.0×10^3 M^{-1} min^{-1} for αV155K. To ensure that equilibrium was approached and to estimate total binding sites, binding in the presence of higher concentrations (50 nM) of ^{125}I-labeled α-bungarotoxin was also measured. Equilibration for αV155K could not be assured, so the rate constant is only an estimate.

α2, α3, and α4 subunits (Figure 1). Because *Nmm*I binding is measured by competition against the initial rate of ^{125}I-labeled α-BgTx binding, the low expression levels may be due to decreased affinity of the long α-toxin, α-BgTx, for the mutant nAChRs. Therefore, we compared rates of association of ^{125}I-labeled α-BgTx for wild-type receptor and the αG153K and αV155K mutant receptors (Figure 3). Binding of the radioligand is slowed by an order of magnitude to the αG153K mutated receptor and by approximately 3 orders of magnitude to the αV155K receptor

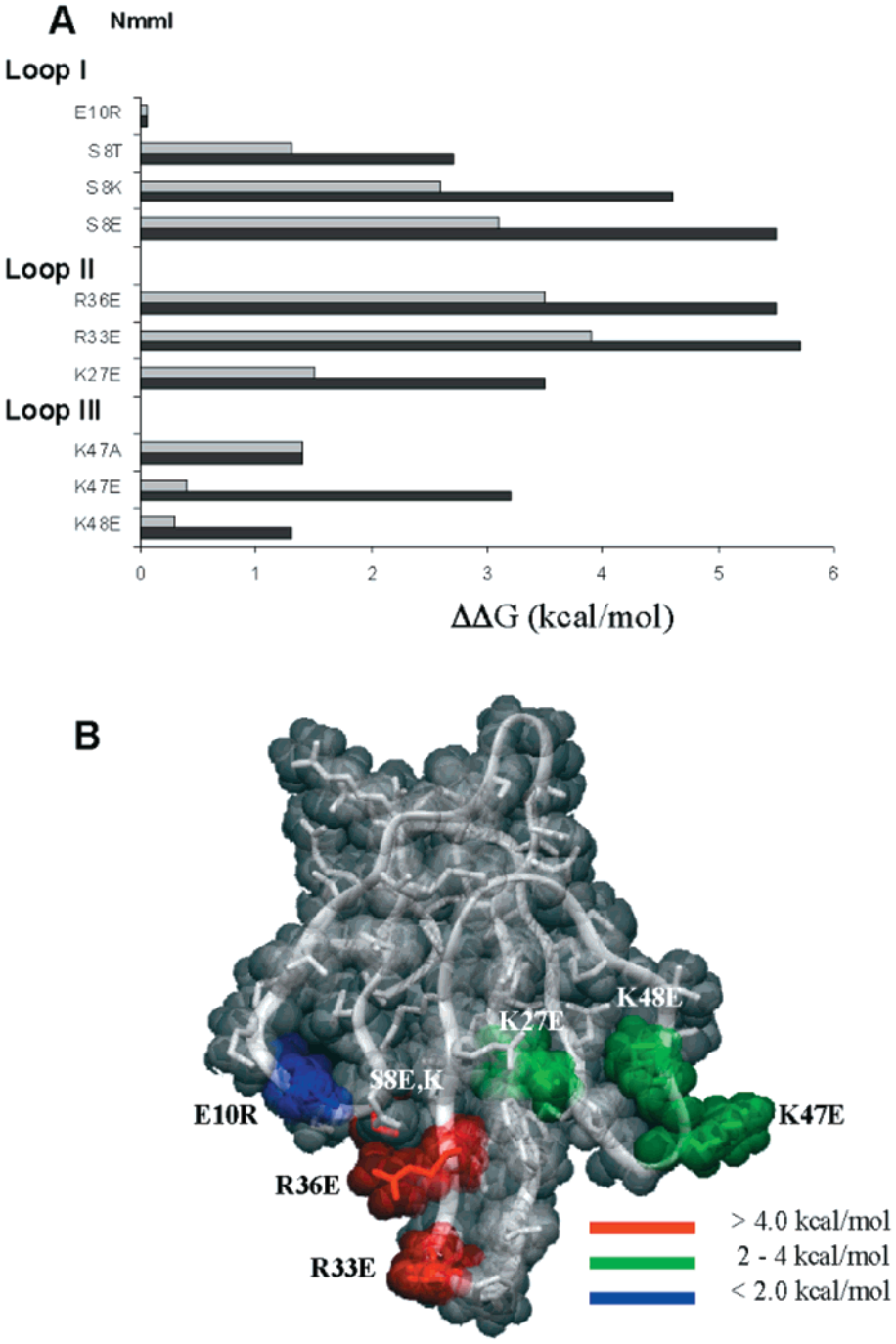

FIGURE 4: Free energy changes associated with mutagenesis of residues in loops I−III of the *Nmm*I α-neurotoxin. (A) ΔΔ*G* values given in Table 1 are compared in the figure for each mutant at the αγ site in black and at the αδ site in gray. The horizontal bars indicate the ratio for wild-type and mutant *Nmm*I. (B) Energy-minimized model of *Nmm*I as described (*14*) is shown with the mutated chains colored according to their energy contribution at the αγ site with wild-type receptor. The concave face of the toxin, which primarily interacts with the receptor residues, is facing the viewer.

as compared to wild-type nAChR. Although, the αG153D and αV155D mutant receptors exhibit low expression, the fractional approach to equilibrium of α-Bgtx association was not appreciably slowed as compared to wild-type receptor (data not shown).

Modification of NmmI α-Toxin Residues. By extending our analysis from the functionally important *Nmm*I residues, Lys[27], Arg[33], and Lys[47] to other point mutations located over the three loops of the α-toxin concave face (Table 1, Figure 4), we are able to define relative energetic contributions in forming the high affinity complex. Reversal of charges on residues proximal to and at the tip of loop II reveals the importance of this loop in stabilizing the *Nmm*I−receptor complex. Both the R36E and R33E mutations decrease affinity by 4 and 3 orders of magnitude at the αγ and αδ sites, respectively (Table 1). The K27E charge reversal, also on loop II but proximal to loop III, decreases affinity by nearly 3 and 1 order of magnitude at the αγ and αδ sites, respectively. The K47E charge reversal on loop III decreases affinity by nearly 40-fold at the αγ site with little loss in affinity at the αδ site. Mutation of Lys[47] to alanine results in equivalent reductions in affinity at the two sites. Charge

reversal of the adjacent lysine, K48E, shows a 10-fold loss in affinity, a change comparable to K47A at the $\alpha\gamma$ site but no significant loss in affinity at the $\alpha\delta$ site.

Two positions on loop I located proximal to loop II were also analyzed for *Nmm*I binding. Charge reversal of E10R did not influence affinity. However, the subtle change from serine to threonine at position 8 decreased affinity at the $\alpha\gamma$ site by 2 orders of magnitude (Table 1). Furthermore, introduction of either a positive or negative side chain at position 8 had a dramatic effect. The S8E mutation produced a decrease in affinity at the $\alpha\gamma$ site comparable to the R33E and R36E mutations.

To confirm that the S8E mutant retained the same secondary structure and disulfide linkages, circular dichroism (CD) experiments in aqueous buffer were conducted. CD spectra of wild-type *Nmm*I and the S8E mutant are superimposable at the same concentrations and possess typical features of both long and short α-neurotoxins: a maximum at 200 nm, a minimum at 214, and a maximum at 228 (data not shown) (*2*).

Double Mutant Cycle Analysis. We then applied thermodynamic mutant cycle analysis to identify pairwise interactions between the α subunit and *Nmm*I and to determine free energy of the individual interactions ($\Delta\Delta G_{INT}$ values in Table 1). Since Columbic or electrostatic forces between point charges are isotropic and can be expected to be exerted over the greatest distances, we have concentrated on charged residue pairs and attempted to reverse the charge orientation between paired residues.

Scheme 1

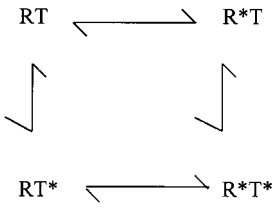

In the mutant cycle shown in Scheme 1, the asterisk indicates the presence of a mutation in either the receptor, R, or the *Nmm*I toxin, T. The loss of energy, $\Delta\Delta G$, arising from substitution from wild type (wt) into mutant (mt) is calculated from the dissociation constant (K_D) as follows:

$$\Delta\Delta G = RT \ln\frac{K_{D,mt}}{K_{D,wt}} \quad (1)$$

The coupling energy, $\Delta\Delta G_{INT}$, is defined in terms of the respective dissociation constants (K_D) of the complexes as follows:

$$\Delta\Delta G_{INT} = RT \ln\frac{K_{R*T*}K_{RT}}{K_{RT*}K_{R*T}} = RT \ln\frac{K_{R*T*}}{K_{RT*}} - RT \ln\frac{K_{R*T}}{K_{RT}} \quad (2)$$

$$\Delta\Delta G_{INT} = (\Delta G^\circ_{R*T*} - \Delta G^\circ_{RT*}) - (\Delta G^\circ_{R*T} - \Delta G^\circ_{RT}) \quad (3)$$

$$\Delta\Delta G_{INT} = (\Delta G^\circ_{R*T*} - \Delta G^\circ_{R*T}) - (\Delta G^\circ_{RT*} - \Delta G^\circ_{RT}) \quad (4)$$

The G° values are standard free energies for formation of the toxin−receptor complex. If the mutations do not interact, the two differences in standard free energies in parentheses will be equal, because the effect of mutating the receptor should be independent of whether the toxin is mutated (eq 3). Similarly, mutating the toxin should be independent of the receptor mutations (eq 4). On the other hand, if the two mutations interact, the parenthetical ΔG differences should not be equal.

Specific pairs of α subunit and *Nmm*I residues, as shown by mutant cycle analysis, contribute significantly to the stabilization of the α-toxin−receptor complex. We focused on six mutation positions in the three α subunit segments (D99R, W149K, V188D, V188K, Y190F, Y190T, Y198E, Y198R, D200K, D200Q) and seven mutation positions in *Nmm*I covering the perimeters of the three toxin loops (E10R, S8E, S8K, K27E, R33E, R36E, K47E, K48E). Table 1 lists the calculated $\Delta\Delta G_{INT}$ values for the $\alpha\gamma$ site. The preferential binding of α-conotoxin MI to the $\alpha\delta$ site (*28*, *29*) was used to distinguish binding at the $\alpha\delta$ and $\alpha\gamma$ sites for the single mutant combinations. In all cases where affinities differed, the $\alpha\gamma$ site was found to be the lower affinity site for *Nmm*I. We have considered interactions determined from mutant cycle analysis to be significant if the average of at least duplicate experiments showed a $\Delta\Delta G_{INT}$ value of $\geq$1.5 kcal/mol. Twenty mutant pairs reveal significant interactions at the $\alpha\gamma$ site. About 75% of the mutant pairs studied show additive contributions, an indication that major conformational changes are not occurring in either the α-toxin or the receptor α subunit due to the specific mutation.

In Table 1, we do not report the $\Delta\Delta G_{INT}$ values measured for the $\alpha\delta$ site. In several cases, the double mutants resulted in such large overall reductions in affinity that it was not possible to distinguish the K_D at the $\alpha\delta$ interface from that at $\alpha\gamma$. α-Conotoxin M1 protection allows one to examine *Nmm*I binding to the $\alpha\gamma$ site without $\alpha\delta$ interference. A more precise approach to analyzing the $\alpha\delta$ site is to conduct the double mutant experiments with receptors expressing the ϵ subunit in place of the γ subunit. As we have previously shown, *Nmm*I binds to the $\alpha\epsilon$ site with 1000-fold lower affinity than to the $\alpha\gamma$ site (*19*). Therefore, changes in K_D for the high affinity site in $\alpha_2\beta\delta\epsilon$ receptors containing an α subunit mutation will be due to shifts in affinity occurring solely at the $\alpha\delta$ site. Coupling energies for the $\alpha\delta$ site will be analyzed in subsequent studies.

Figure 5 illustrates the strong interaction between receptor residue αVal^{188} with α-toxin residue Arg^{36} as determined by mutant cycle analysis. Insertion of a positive charge at α188 increased the K_D for *Nmm*I by 2 orders of magnitude at the $\alpha\gamma$ site. The *Nmm*I toxin mutation, R36E, increased the K_D for receptor by 4 orders of magnitude. When the αV188K mutant receptor and R36E mutant toxin are combined, rather than achieving a K_D reflecting the product of the increase in dissociation constants for the singly mutated complexes (i.e., an increase in K_D greater than 10^6), the K_D increased by only 10^4. Hence, charge reversal in the toxin residue partner restores an affinity equivalent to 3.4 kcal/mol to the α-toxin−receptor complex, reflecting the contribution of a strong electrostatic interaction between charged side chains on residue α198 and *Nmm*I residue 36.

Interactions of Receptor Residue α-Tyr[198] with α-Toxin Residue Ser[8]. In addition to the αV188K and R36E pair, a similar interaction is evident between residues at position 8

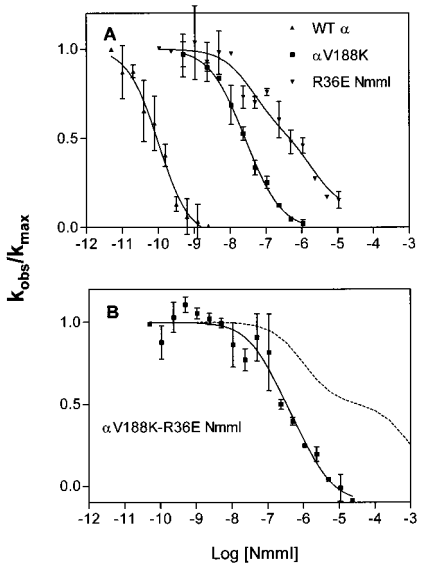

FIGURE 5: Free energy of binding determined by mutant cycle analysis after sequential residue modification on *Nmm*I α-toxin and the α subunit of nAChR. (A and B) 293 HEK cells were transfected with cDNAs encoding wild-type α or αV188K subunits, along with cDNAs for *β*-, *γ*-, and *δ* subunits and binding of wild-type or R36E *Nmm*I was determined. The dashed line in panel B is the predicted curve when the coupling energy ($\Delta\Delta G_{INT}$) between αV188K and R36E is zero. The deviation of observed affinity (B) from the predicted by no coupling (dashed line) produces a large coupling energy of −3.4 kcal/mol. Binding determinations for *Nmm*I toxins were measured as the fractional reduction in the initial rates of ^{125}I-labeled α-bungarotoxin binding in the absence of *Nmm*I (k_{max}) or in the presence of the indicated amounts of *Nmm*I (k_{obs}). The curves for the wild-type *Nmm*I−wild-type nAChR are least-squares fits to the Hill equation with $n_H = 1.0$. The remaining curves are least-squares fits to two binding sites present in equal populations.

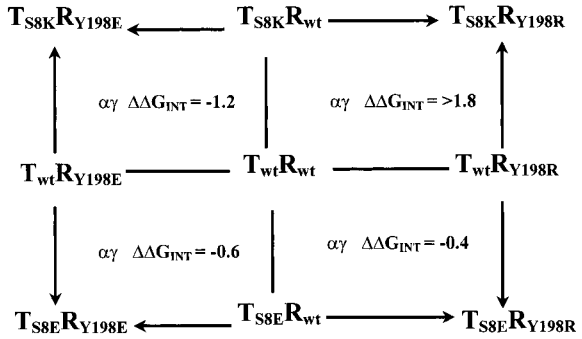

FIGURE 6: Network of mutant cycles between toxin (T) position 8 with receptor (R) position 198. The changes in binding affinity with each mutant are shown within each small square for the α*δ* and α*γ* sites. $\Delta\Delta G_{INT}$ values are in kilocalories per mole. The overall coupling energy for K8E/E198R was calculated for the double mutant combinations shown in bold at the corners of the large square. At the α*γ* site, $\Delta\Delta G_{INT} = -2.8$ kcal/mol. K8E/E198R produces particularly large coupling energies at the two interfaces presumably because of the enhancement of binding affinity produced by charge reversing the mutations.

on the α-toxin with position 198 on the α subunit. Native residues at both positions are neutral. At each position we constructed positive and negative mutations. Figure 6 shows the network of mutations to achieve the charge reversals of K8E/E198R for the interacting pairs of α-toxin and α subunit mutations. Four separate mutant cycles are shown with the energy of interaction for each cycle.

The Y198E/S8E or Y198E/S8K double mutant combinations result in 4 and 5 orders of magnitude decreases in affinity at the α*γ* site (Table 1). Furthermore, the Y198R mutation when paired with either S8E or S8K on the α-toxin greatly destabilizes the complex resulting in K_D values in the millimolar range, exceeding the practical limits of our experimental conditions. Assuming shifts of 10^6- and 10^7-fold for the combination of double mutant pairs Y198R/S8E and Y198R/S8K, respectively, we calculated the overall binding energy for the double charge reversal combination, K8E/E198R. The central point in the network, the wild type−wild type pair of neutral residues, represents an intermediate state to charge reversal. K_D values for the double mutant combinations, representing the four corners of the network, were used to calculate the coupling energy for the overall cycle. Nearly 3.0 kcal/mol stabilization energy results at the α*γ* site when conversion of positive to negative charge at position 8 on the α-toxin is paired with conversion of negative to positive charge at position 198 on the α subunit. We also constructed and analyzed a similar mutant cycle for the overall charge reversion of the K8E/D188K. In this case, no pairwise interaction is detected between position 8 on the α-toxin and position 188 on the α subunit. This reveals a localized interaction of loop I with the relatively large binding surface encompassed by segment C.

Coupling Analysis for Paired Residues Based on Charge Reversal. Results from double mutant cycle analysis for the seven toxin positions all involving charge reversal are reported in Figure 7A. We present the data with the toxin mutations in the sequence as they are arranged spatially on the concave face of the α-toxin, starting from loop I to loop III. In addition, we report the coupling energies as negative or positive $\Delta\Delta G_{INT}$ values. Since we have reversed charges on both the toxin and α subunit residues and have analyzed overall charge reversal, directionality of the coupling energies provides an indication as to whether the interaction results in enhanced destabilization of the complex due to repulsion between the residues in question (positive $\Delta\Delta G_{INT}$ values) or results in increased stabilization of the complex dominated by attractive forces (negative $\Delta\Delta G_{INT}$ values).

We have focused on four positions on the α subunit that involve charge reversal: D99R, D188K, E198R, and D200K (Figure 7A). At the α*γ* site, the D99R/K48E and the D200K/R33E mutant pairs both display coupling energies of −2.0 to −2.5 kcal/mol. The strongest pairwise interactions for overall charge reversal mutations are observed for D188K and E198R on the α subunit. Results for D188K highlight the importance of the three loop II residues: Arg^{36}, Arg^{33}, and Lys^{27}. R36E shows significant attractive coupling energy of −3.4 kcal/mol when a positive charge is inserted at α188 at the α*γ* site. This attractive coupling energy drastically diminishes to −0.9 kcal/mol with conversion to a negative charge at α188. The energetic components combined for the D188K/R36E pair translate into an overall coupling energy of −2.4 kcal/mol. Results for R36E yielded values similar to our previous calculated results for the D188K/R33E mutant pair, which displays −3.0 kcal/mol coupling energy (*15*). The D188K/K27E charge reversal mutations result in a modest, −1.6 kcal/mol coupling energy at the α*γ* interface. Mutant cycle analysis for E198R is dominated by the large energetic change at the α*γ* site (∼3.0 kcal/mol attractive energy) for charge reversal at α-toxin position 8 as mentioned above and shown in Figure 6. R33E does show significantly enhanced coupling energy of −3.0 kcal/mol when a positive

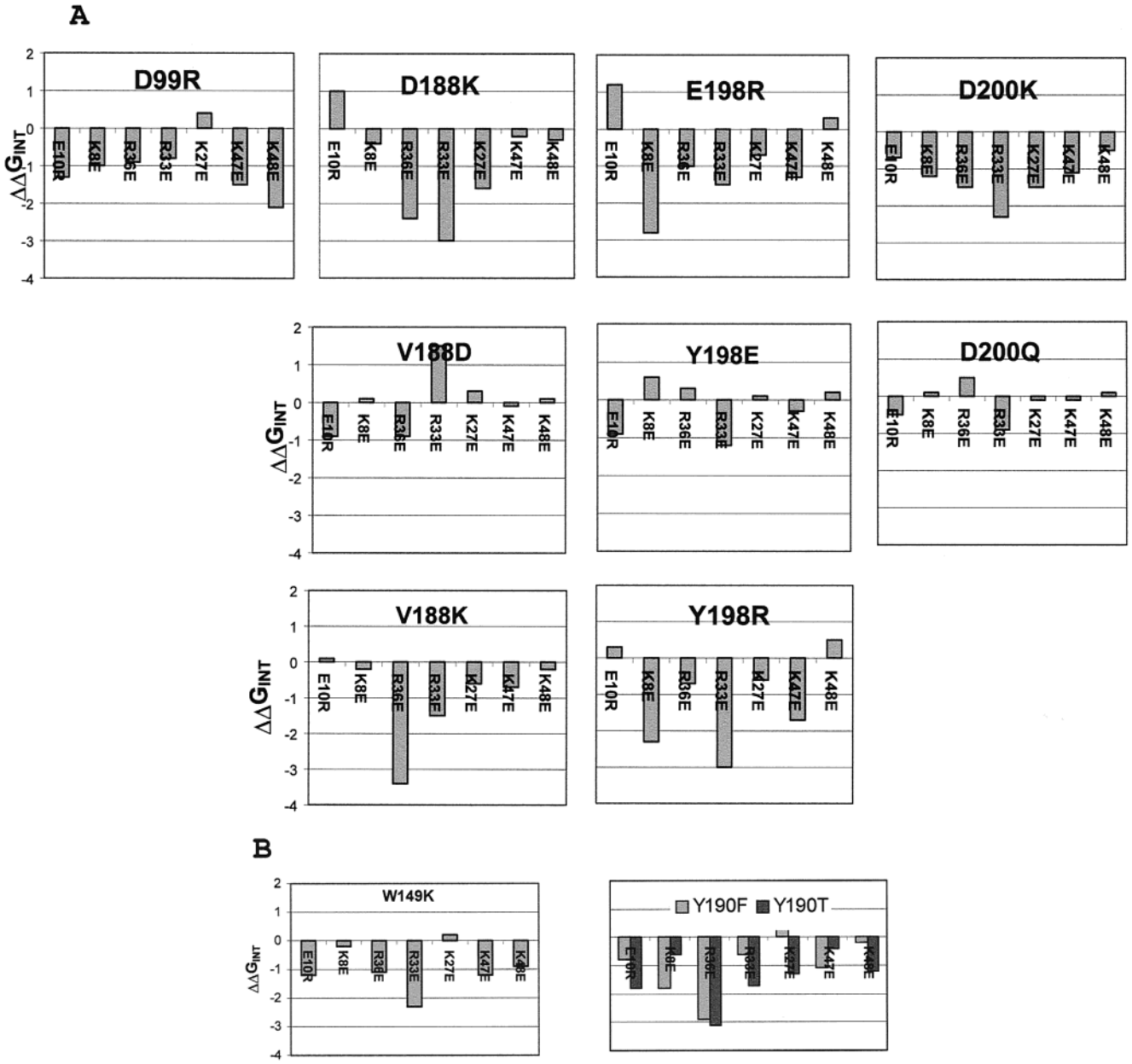

FIGURE 7: Analysis of the network mutant cycles for the $\alpha\gamma$ site (Scheme 1). (A) The residue positions in the α subunit are converted from negative to positive side chains. The α-toxin mutations invert the charge at the respective positions on the native toxin. The sequence reflects the spatial positions of the residues extending from loop I to loop III. The neutral frames of reference are the residues (Val199 and Tyr198) in the wild-type receptor. (B) α subunit mutations that do not involve charge reversal. $\Delta\Delta G_{INT}$ values are determined as described by eqs 2−4.

charge is inserted at α198, similar to the V188K/R36E analysis. On the other hand, −1.2 kcal/mol coupling energy is retained when a negative charge is inserted at α198 and paired with R33E. The diminished repulsion observed for the Y198E/R33E pair as compared to the large attraction observed for the Y198R/R33E double mutant involving charge reversal translates into only modest coupling of −1.5 kcal/mol for the overall E198R/R33E pair.

We likewise investigated two positions on the α subunit that do not involve charge reversal (Figure 7B). R33E shows an electrostatic attraction of −2.3 kcal/mol coupling energy at the $\alpha\gamma$ site when paired with αW149K. We previously reported results for the four double mutant combination involving αY190F and αY190T with toxin mutants K27E and R33E (*15*). Here, we show that the R36E mutant shows the greatest interaction energy at the $\alpha\gamma$ site (∼−3.0 kcal/mol) upon removal of an aromatic hydroxyl at the α190 position.

DISCUSSION

Our investigation seeks to define further the molecular architecture of the nicotinic receptor by studying its high affinity interaction with an α-neurotoxin of known structure. Studies of other peptide−protein interactions with comparable affinities and of known structure, such as fasciculin 2-acetylcholinesterase (*7*), barnase−barnstar (*16*), and human growth hormone and its receptor (*30*), indicate that up to 30 residues on the receptor may be within van der Waals radii contact with the α-toxin, but only a fraction of these residues contribute significantly to the binding energy.

Of the several residues we have found to be determinants on the α-toxin and α subunit, greater losses of affinity occur at the αγ site upon modification of the α subunit relative to the αδ site (Figures 2 and 4). The αY198R substitution is the one exception and displays equal affinity changes for α-toxin at both the αδ and αγ sites upon mutagenesis. The results suggest that more of the stabilization energy for binding the nAChR−*Nmm*I complex is contributed from the δ subunit interface than the γ interface at the respective αδ and αγ sites. The smaller losses in affinity at the αδ site may indicate an accessibility difference of the two binding sites by α-toxin as postulated by Sáez-Briones et al. (*31*). Their work involving derivatization of an α-toxin with bulky cross-linking reagents suggests that the αδ site possesses fewer steric constraints than the αγ site. Since our analysis emphasizes charged residues, it is also possible that αγ stabilization of the complex is conferred mainly by electrostatic interactions, but αδ is dominated by hydrophobic interactions. The findings also suggest that the orientations of the toxin loops differ when bound at the αδ and αγ interfaces.

Our mutagenesis scan of the α1 subunit also revealed that addition of charged residues in segment B reduces affinity of the α-neurotoxin−receptor complex. Probably, specific cationic side chains in this region for the α2, α3, and α4 subunits prevent binding of the short and long α-neurotoxins to the neuronal nicotinic receptor (Figure 1).

Relative Pairwise Proximities Based on Electrostatic Interactions. To identify residues on the α subunit and the α-toxin involved in pairwise recognition, we determined the energetic contributions for *Nmm*I binding of individual mutations in the α subunit by thermodynamic mutant cycle analysis. The resulting $\Delta\Delta G_{INT}$ values obtained are composed of both electrostatic and nonelectrostatic contributions. By focusing on mutant pairs involving overall charge reversal, we highlight the relative electrostatic forces between the pairs in question. Furthermore, relative proximities between the residue pairs can be estimated from the $\Delta\Delta G_{INT}$ values.

Schreiber and Fersht (*16*) provide a correlation between $\Delta\Delta G_{INT}$ values obtained from mutant cycle analysis and actual distances based on the crystal structure of the barnase−barnstar complex. Coulomb's law has also been used to translate electrostatic energies into distances between ion pairs in macromolecules (*32*). Chang et al. (*33*) used this formulism and a standard dielectric constant to calculate interactions between a cone snail toxin and the muscle Na^+ channel. By either method, interaction energies between 1.0 and 1.5 kcal/mol translate into interresidue distances of 5−8 Å. Energy values between 2.0 and 4.0 kcal/mol are in the range of 3−5 Å and values ≥4.0 kcal/mol indicate a close range interaction, approximately 2−3 Å separation. Thus, the relationship between $\Delta\Delta G_{INT}$ values and proximities of paired residues provides a basis for grouping interacting residue pairs in the toxin−receptor complex into spatial regions according to the extent of their energetic interactions. Rank ordering of these interactions should provide a more comprehensive view of the α-toxin−receptor complex and further refinements of proposed model structures of the receptor (*13*, *34*).

Subunit Contributions to NmmI Binding. Our initial studies of the nAChR−*Nmm*I complex using double mutant cycles revealed pairwise contacts between residues on the central loop of *Nmm*I and the α subunit residues Val^{188}, Tyr^{190}, and Asp^{200} (*15*). We have extended those studies to incorporate all three loops of the α-toxin and three domains of the α subunit and present an overall network mutant cycle analysis of the α subunit in Figure 7. These combined $\Delta\Delta G_{INT}$ energies enable us to ascertain a preliminary orientation of the α-toxin with respect to the αγ interface. Figure 8 shows the proposed locations of α subunit residues and γ subunit residues in relation to α-toxin residues based on coupling energies determined for the multiple residue pairs.

NmmI Interaction with the αγ Site. Figure 8A displays linkages determined for the α subunit at the αγ site. $\Delta\Delta G_{INT}$ values reveal that Arg^{33} significantly interacts with αVal^{188} as well as with αTrp^{149} and αAsp^{200} (Figure 7A). These results suggest that the tip of loop II is a central contact point within the triad of α residues. A toxin residue three residues carboxy terminal from Arg^{33} on loop II, Arg^{36} likewise shows strong coupling with αVal^{188} and, in addition, links strongly with αTyr^{190}. Ser^8 on loop I, on the other hand, is highly influenced by the tyrosine at α198. Approximately, 12 Å separates the α carbons on Ser^8 and Arg^{36} of *Nmm*I based on the crystal structure of Ea (*22*). Here, we provide evidence for positioning of the nearby tyrosines, Tyr^{190} and Tyr^{198}, within this 12-Å gap between loops I and II of *Nmm*I in the bound complex. NMR studies of α-BgTx complexed with a short peptide mimicking the region 187−200 of the α subunit previously indicated that this segment is positioned between the first two loops of the long α-toxin (*35*, *36*). Convincing support is provided by the cysteine cross-linking results of Michalet and co-workers (*23*) that position the α thiols: Cys^{192}−Cys^{193} between loops I and II in the short α-toxin from *Naja nigricollis* framed by residues Gln^{10}, Trp^{29}, and Arg^{33}.

Lys^{27} interacts modestly with α188 and α200 side chains as shown in the charge reversal experiments, but otherwise, no significant linkages are observed for this α-toxin residue and the α subunit residues, supporting the proximity of Lys^{27} to the γ subunit. Likewise, Michalet et al. (*23*) report very low cross-linking reactivity between cysteine derivatives K27C and K47C in *N. nigricollis* with αCys^{192}-Cys^{193}. We observe moderate coupling of Lys^{47} with charge reversal at α99 and slightly larger coupling with Lys^{48} suggesting that loop III of the α-toxin points away from the binding crevice encompassing α residues, 186−200, but is somewhat closer to segment A.

Figure 8B displays linkages determined for the γ subunit (*19*). We reported large coupling energies between Arg^{33} at the tip of loop II and γLeu^{119} (−5.7 kcal/mol) and between Lys^{27} and γGlu^{176} (−5.9 kcal/mol). Also, Trp^{55} at the γ interface, couples strongly to both Arg^{33} and Lys^{27}. Lys^{47} couples only modestly with γAsp^{174}; otherwise other charged α-toxin residues show insignificant linkages with this residue. Earlier cross-linking studies positioned γAsp^{174} ∼9 Å from the disulfide at αCys^{192}−Cys^{193} (*37*). Thus, our combined results are complementary to those of Michalet et al. (*23*) and strongly suggest that Lys^{27} and Lys^{47} approach residues on the γ (or δ) binding face more closely than α residues 186−200.

The combined information of Figure 8A,B highlights that Arg^{33} of *Nmm*I couples strongly to both αVal^{188} and γLeu^{119}, suggesting the proximity of these two residues on opposing faces of the αγ interface where Arg^{33} bisects the two

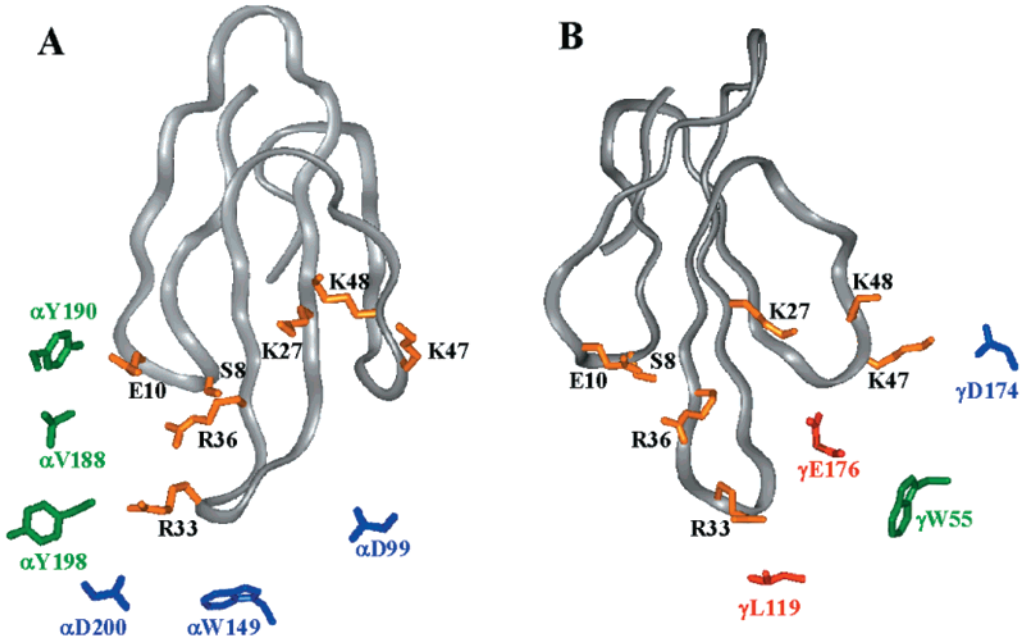

FIGURE 8: Observed pairwise interactions at the $\alpha\gamma$ interface. In cases where charge reversal is analyzed (residues 99, 188, 198, and 200 in the α subunit and residues 55, 119, 174, and 176 in the γ subunit), the residues are positioned to reflect intersite distances between charged atoms on the respective side chains. In the remaining cases, W149 and Y190, the positions reflect intersite distances between side chains on the wild-type α-toxin and receptor. Although a precise distance representation is not possible in two dimensions, residue positions reflect the $\Delta\Delta G_{INT}$ values shown in Table 1. Red residues $\Delta\Delta G_{INT}$ >4.0 kcal for the most proximal residue; green residues, $\Delta\Delta G_{INT}$ = 2.5−4.0 kcal, blue, 1.5−2.5 kcal. (A) relation between *Nmm*I and the α subunit residues at the $\alpha\gamma$ site. The concave surface of *Nmm*I is facing the viewer and is offset from center by 45 deg to the left. (B) Relation between *Nmm*I and the γ subunit residues. The concave surface of *Nmm*I is facing the viewer and is offset from center by 45 deg to the right. The $\Delta\Delta G_{INT}$ values for the γ subunit are found in ref *20*.

subunits. Other examples exist supporting the proximity of the subunit fragments. Besides the measured distance of ∼9 Å between αCys[192]−Cys[193] and δAsp[180] or γAsp[174] determined by Czajkowski and Karlin (*37*), Utkin et al. (*38*) report a 13-Å distance between α and δ or α and γ subunits based on cross-linking studies of a long α-neurotoxin derivatized at loop II. In addition, Fu and Sine (*39*) showed that one quaternary group of dimethyl-*d*-tubocurarine interacts directly with Tyr[198] on the α subunit and the second group, 10.8 Å away, interacts with Tyr[117] on the γ subunit. Our data also reveal that Lys[27] in *Nmm*I links directly with γGlu[176] but to a lesser extent with αVal[188]. Both Arg[33] and Lys[27] couple modestly with αTyr[190] and γTrp[55]. Arg[36], on the other hand, links strongly to αTyr[190] as well as to αVal[188] and does not partner with any γ subunit residues. Ser[8] likewise interacts with the α subunit predominately by linking to αTyr[198].

Thus, Arg[33] which is at the tip of loop II anchors the α-toxin to both the α and γ subunit surfaces, whereas the portion of loop II extending in the amino terminal direction (Lys[27]) interacts with the γ subunit and the portion extending in the carboxy terminal direction (Arg[36]), along with loop I residues interacts with the α subunit.

Having established that the concave surface of the short α-neurotoxins interacts with the receptor surface (*5*, *15*), then toxin structure can be used to predict handedness of receptor subunit order around the pentamer. Should the toxin molecule interdigitate between the subunit interfaces from the outer perimeter of the receptor, the tips of the three loops angle toward the membrane and the central channel, and the concave surface orient away from the membrane, then a clockwise circular order of $\alpha\gamma\alpha\delta\beta$ from the extracellular side, as suggested by Hucho and colleagues (*40*), would be predicted. Should the concave surface be oriented toward the membrane and the other conditions apply, then the clockwise order of $\alpha\gamma\alpha\beta\delta$, arbitrarily selected in Tsigelny et al. (*13*), would apply. Should the toxin enter the receptor from the channel vestibule at the apex of the receptor and the concave toxin surface interact with the channel vestibule lining, then the $\alpha\gamma\alpha\beta\delta$ clockwise order would also apply. On the basis of the dimensions of the toxin and the vestibule and the often observed equivalence of association rates for the toxin molecules at the two sites, the vestibular portal of α-toxin entry seems unlikely.

Determination of pairwise interactions at the $\alpha\delta$ site in relation to interactions at the $\alpha\gamma$ site constitutes the next step in our analysis of α-neurotoxin positioning at the subunit interfaces of nAChR. Hydrophobic forces may prevail at the $\alpha\delta$ interface, whereas electrostatic interactions play a diminished role. Tryptophan at position 29 in *Nmm*I is highly conserved in the family of curaremimetic toxins. Mutagenesis studies with Ea, *N. nigricollis*, and α-cobratoxin have suggested that Trp[29] (*Nmm*I numbering) plays a significant role in the association predominately due to its aromaticity (*6*, *22*, *23*). In addition, Lys[47] and to a lesser extent Lys[27] show large repulsive interactions with a cluster of α residues specifically at the $\alpha\delta$ site (unpublished results). The lack of interactions of these two residues at the $\alpha\gamma$ site suggests a selective role in stabilizing the α-toxin at δ subunit face of the $\alpha\delta$ site.

Affinity labeling and site-specific mutagenesis (for reviews see refs *12*, *13*, *41*, and *42*), identification of antibody sites (*21*, *43*), molecular dynamics modeling (*13*, *34*), and electron microscopy reconstruction analysis (*44*) all have contributed to the development of a low resolution structure of the

nAChR. Homology modeling of the extracellular domains of the individual subunits of the nAChR based on copper binding proteins of known crystal structure enabled us to propose a repeating hairpin domain for a central region of the α subunit extending between residues 31 and 164 (*13*). This folding pattern can be refined as residues are identified on the two complementary faces of the α and γ subunits that contribute to binding *Nmm*I. The high affinity of the α-toxin permits its interaction with the receptor to be studied in detail by mutant cycle analysis. Lower affinity ligands lack a sufficient window of specificity to permit the quantitation of successive reductions of affinity upon mutation of both the ligand and receptor. Hence, the selectivity and high affinity arising from the large surface areas of contact in two subunits have allowed us to orient the α-toxin in relation to several residues forming the surface of the binding site at the subunit interface.

ACKNOWLEDGMENT

We thank Dr. Pascale Marchot, Laboratoire de Biochimie, Institut Federatif de Recherche, Jean Roche, Universite de la Mediterranee, Marseille, France, for the generous gift of purified *Nmm*I α-toxin.

REFERENCES

1. Changeux, J.-P., Kasai, M., and Lee, C. Y. (1970) *Proc. Natl. Acad. Sci. U.S.A. 67*, 1241−1245.
2. Endo, T., and Tamiya, N. (1987) *Pharmacol. Ther. 14*, 403−451.
3. Changeux, J.-P., and Edelstein, S. J. (1998) *Neuron 21*, 959−980.
4. Endo, T., and Tamiya, N. (1991) in *Snake Toxins* (Harvey, A. L., Ed.) pp 259−302, Pergamon Press, New York.
5. Servant, D., Winckler-Dietrich, V., Hu, H., Kessler, P., Drevet, P., Bertrand, D., and Ménez, A. (1997) *J. Biol. Chem. 272*, 24279−24286.
6. Trémeau, O., Lemaire, C., Drevet, P., Pinkasfeld, S., Ducancel, F., Boulain, J. C., and Ménez, A. (1995) *J. Biol. Chem. 270*, 9362−9369.
7. Bourne, P., Taylor, P., and Marchot, P. (1995) *Cell 83*, 503−512.
8. Harel, M., Kleywegt, G. J., Revelli, R. B., Silman, I., and Sussman, J. L. (1995) *Structure 3*, 1355−1366.
9. Marchot, P., Frachon, P., and Bougis, P. E. (1988) *Eur. J. Biochem. 174*, 537−542.
10. Unwin, N. (1993) *J. Mol. Biol. 229*, 1101−1124.
11. Karlin, A., and Akabas, M. H. (1995) *Neuron 15*, 1231−1244.
12. Hucho, F., Tsetlin, V. I., and Machold, J. (1996) *Eur. J. Biochem. 239*, 539−557.
13. Tsigelny, I., Sugiyama, N., Sine, S. M., and Taylor, P. (1997) *Biophys. J. 73*, 52−66.
14. Ackermann, E. J., and Taylor, P. (1997) *Biochemistry 36*, 12836−12844.
15. Ackermann, E. J., Ang, E. T.-H., Kanter, J. R., Tsigelny, I., and Taylor, P. (1998) *J. Biol. Chem. 273*, 10958−10954.
16. Schreiber, G., and Fersht, A. R. (1995) *J. Mol. Biol. 248*, 478−486.
17. Hidalgo, P., and MacKinnon, R. (1995) *Science 268*, 307−310.
18. Ranganathan, R., Lewis, J. H., and MacKinnon, R. (1996) *Neuron 16*, 131−139.
19. Osaka, H., Malany, S., Kanter, J. R., Sine, S. M., and Taylor, P. (1999) *J. Biol. Chem. 274*, 9581−9586.
20. Osaka, H., Malany, S., Molles, B. M., Sine, S. M., and Taylor, P. (2000) *J. Biol. Chem. 275*, 5478−5484.
21. Ducancel, F., Mérienne, K., Fromen-Romano, C., Trémeau, O., Pillet, L., Drevet, P., Zinn-Justin, S., Boulain, J.-C., and Ménez A. (1996) *J. Biol. Chem. 271*, 31345−31353.
22. Antil, S., Servant, D., and Ménez A. (1999) *J. Biol. Chem. 274*, 34851−34858.
23. Michalet, S., Teixeira, F., Gilquin, B., Mourier, G., Servant, D., Dervet, P., Binder, P., Tzartos, S., Ménez A., and Kessler, P. (2000) *J. Biol. Chem. 275*, 25608−25615.
24. Sine, S. M., and Taylor, P. (1981) *J. Biol. Chem. 256*, 6692−6699.
25. Sine, S. M., and Taylor, P. (1979) *J. Biol. Chem. 254*, 3315−3325.
26. Sugiyama, N., Boyd, A. E., and Taylor, P. (1996) *J. Biol. Chem. 271*, 26575−26581.
27. Luetje, C. W., Maddox, F. N., and Harvey, S. C. (1998) *Mol. Pharmacol. 53*, 1112−1119.
28. Kreienkamp, H.-J., Sine, S. M., Maeda, R. K., and Taylor, P. (1994) *J. Biol. Chem. 269*, 8108−8114.
29. Sine, S. M., Kreienkamp, H.-J., Bren, N., Maeda, R. K., and Taylor, P. (1995) *Neuron 15*, 205−211.
30. Vijayakumar, M., Wong, K.-Y., Schreiber, G., Fersht, A. R., Szabo, A., and Zhou, H.-X. (1997) *J. Mol. Biol. 278*, 1015−1024.
31. Sáez-Briones, P., Krauss, M., Dreger, M, Herrmann, A., Tsetlin, V., and Hucho, F. (1999) *Eur. J. Biochem. 265*, 902−910.
32. Warshel, A. (1991) *Annu. Rev. Biophys. Chem. 20*, 267−298.
33. Chang, N. S., French, R. J., Lipkind, G. M., Fozzard, H. A., and Dudley, S., Jr. (1998) *Biochemistry 37*, 4407−4419.
34. Le Novere, N., Corringer, P.-J., and Changeux, P. (1999) *Biophys. J. 76*, 2329−2345.
35. Basus, V. J., Song, G., and Hawrot, E. (1993) *Biochemistry 32*, 7231−7241.
36. Scherf, T., Balass, M., Fuchs, S., Katchalski-Katzir, E., and Anglister, J. (1997) *Proc. Natl. Acad. Sci. U.S.A. 94*, 6059−6064.
37. Czajkowski, C., and Karlin, A. (1995) *J. Biol. Chem. 270*, 3160−3164.
38. Utkin, Y. N., Krivoshein, A. V., Davydov, V. L., Kasheverov, I. E., Franke, P., Maslennikov, I. V., Arseniev, A. S., Hucho, F., and Tsetlin, V. I. (1998) *Eur. J. Biochem. 253*, 229−235.
39. Fu, D.-X., and Sine, S. (1994) *J. Biol. Chem. 269*, 26152−26157.
40. Machold, J., Weise, C., Utkin, Y., Tsetlin, V., and Hucho, F. (1995) *Eur. J. Biochem. 234*, 427−430.
41. Arias, H. R. (2000) *Neurochem. Int. 36*, 595−645.
42. Corringer, P.-J., Le Novere, N., and Changeux, J.-P. (2000) *Annu. Rev. Pharmacol. Toxicol. 40*, 431−458.
43. Unwin, N. (1995) *Nature 373*, 37−43.
44. Miyazawa, A., Fujiyoshi, Y., Stowell, M., and Unwin, N. (1999) *J. Mol. Biol. 288*, 755−786.

BI001825O